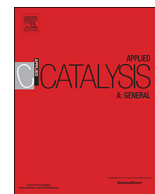




ELSEVIER

Contents lists available at ScienceDirect

## Applied Catalysis A, General

journal homepage: [www.elsevier.com/locate/apcata](http://www.elsevier.com/locate/apcata)Effect of molybdenum on the structure and performance of V<sub>2</sub>O<sub>5</sub>/TiO<sub>2</sub>-SiO<sub>2</sub>-MoO<sub>3</sub> catalysts for the oxidative degradation of *o*-chlorotolueneRyoji Kuma<sup>a,\*</sup>, Tomoyuki Kitano<sup>b</sup>, Takuya Tsujiguchi<sup>a</sup>, Tsunehiro Tanaka<sup>c,d</sup><sup>a</sup> Catalysts & Green Energy Materials Research Department, Nippon Shokubai Co. Ltd., 992-1 Aza-Nishioki, Okinohama, Aboshi-ku, Himeji, Hyogo, 671-1292, Japan<sup>b</sup> Analysis Technology Center, Nippon Shokubai Co. Ltd., 5-8, Nishi Otabi-cho, Suita, Osaka, 564-0034, Japan<sup>c</sup> Department of Molecular Engineering, Graduate School of Engineering, Kyoto University, Kyoto, 615-8510, Japan<sup>d</sup> Elements Strategy Initiative for Catalysts and Batteries (ESICB), Kyoto University, Kyoto, 615-8510, Japan

## ARTICLE INFO

## Keywords:

V<sub>2</sub>O<sub>5</sub>/TiO<sub>2</sub>-SiO<sub>2</sub>-MoO<sub>3</sub>*o*-Chlorotoluene

XAFS

## ABSTRACT

V/TiO<sub>2</sub>-SiO<sub>2</sub>-MoO<sub>3</sub> (TSM) catalysts exhibit enhanced redox capabilities, but the role of each species in the mixed oxide support is not well understood. Herein, the physicochemical characteristics of molybdenum oxide in TSM were investigated using X-ray diffraction, X-ray photoelectron spectroscopy, and X-ray absorption fine structure spectroscopy, and the performance of V/TSM catalysts for the oxidative decomposition of *o*-chlorotoluene was examined. The V/TSM catalysts exhibited superior performances in this decomposition reaction at low temperatures. The molybdenum species were highly dispersed as Mo<sup>6+</sup>, replacing Ti<sup>4+</sup> in the anatase TiO<sub>2</sub> framework and forming a solid solution. The redox capability of the vanadium species in the catalyst was enhanced by electron transfer from the TSM support to vanadium, likely due to the coexistence of Mo<sup>6+</sup> and Ti<sup>4+</sup> in the TSM solid solution, which has a unique structure. These results are expected to contribute to enhancing the abatement of dioxins at low temperatures.

## 1. Introduction

Flue gases from municipal waste incineration processes commonly contain harmful NO<sub>x</sub> gases (NO, NO<sub>2</sub>) and toxic dioxins, such as polychlorinated dibenzo-*p*-dioxins and polychlorinated dibenzofurans. As such, the catalytic degradation of these pollutants has been intensively investigated, with the decomposition of NO<sub>x</sub> and NH<sub>3</sub> being commonly carried out industrially over selective catalytic reduction (SCR) catalysts such as V<sub>2</sub>O<sub>5</sub>/TiO<sub>2</sub> [1–6]. As V<sub>2</sub>O<sub>5</sub>/TiO<sub>2</sub> catalysts are also capable of decomposing dioxins, they have been applied for the simultaneous abatement of NO<sub>x</sub> and dioxins discharged from municipal waste incinerators [7–15]. Generally, an electrostatic precipitator or a fabric filter is used for such processes (Fig. 1), the latter of which is known to collect fly ash more effectively [16]. However, owing to the low heat resistance of fabric filters, the gas temperature should be lower than 150 °C in most cases. Subsequently, the outlet gas from the fabric filter requires reheating to a higher temperature to achieve the catalytic decomposition of both NO<sub>x</sub> and dioxins. Although a higher catalytic activity can be achieved at higher temperatures, a large amount of energy is required for the reheating process.

Highly active catalysts are therefore necessary for low-temperature dioxin decomposition and in particular for the fabric filter process.

Nevertheless, few reports exist concerning the catalytic decomposition of dioxins at temperatures lower than 200 °C. Although WO<sub>3</sub> or MoO<sub>3</sub> has conventionally been added to promote the activity and SO<sub>2</sub> durability of V<sub>2</sub>O<sub>5</sub>/TiO<sub>2</sub> catalysts [7,8,10,12], these catalysts require temperatures higher than 250 °C to realize satisfactory dioxin decomposition efficiencies.

In this context, we previously developed a V<sub>2</sub>O<sub>5</sub>/TiO<sub>2</sub>-SiO<sub>2</sub>-MoO<sub>3</sub> (V/TSM) catalyst with high activity for low-temperature NH<sub>3</sub>-SCR [17]. The mixed oxide support material of this catalyst, TSM, was prepared via a coprecipitation method. As the activity of the V/TSM catalyst was found to be enhanced by its redox capability, the activity would be expected to be improved for the oxidative decomposition of dioxins. However, the role of the TSM support material and the mechanism of redox enhancement require clarification to allow optimization of its composition to obtain a superior catalytic performance.

Thus, we herein report our study into the physicochemical characteristics of molybdenum oxide in V/TSM catalysts. Catalytic activity tests were carried out using *o*-chlorotoluene as a substitute for dioxins due to the high toxicity of dioxins and the similar decomposition behavior of *o*-chlorotoluene [18]. The structure–activity relationships for the V/TSM catalysts were investigated using Mo K-edge X-ray absorption near-edge structure (XANES) and X-ray absorption fine structure

\* Corresponding author.

E-mail address: [ryoji\\_kuma@shokubai.co.jp](mailto:ryoji_kuma@shokubai.co.jp) (R. Kuma).<https://doi.org/10.1016/j.apcata.2020.117496>

Received 5 November 2019; Received in revised form 26 February 2020; Accepted 29 February 2020

Available online 29 February 2020

0926-860X/ © 2020 Elsevier B.V. All rights reserved.

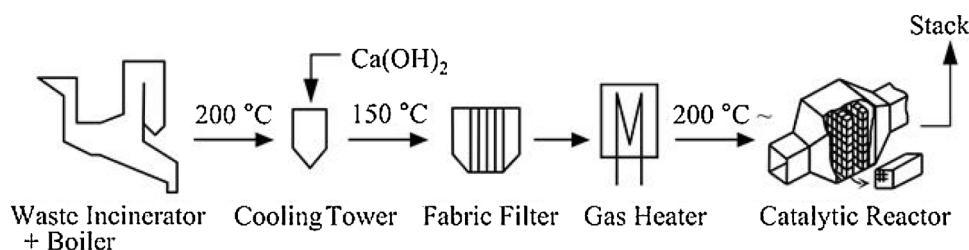


Fig. 1. Catalytic dioxin decomposition process in municipal waste incineration plants.

(EXAFS) spectroscopy. XANES spectroscopy provides information regarding the local geometry around the absorbing atom and its oxidation state, whereas EXAFS spectroscopy is a powerful technique for obtaining direct structural information.

## 2. Experimental

### 2.1. Catalyst preparation

TSM mixed oxides were prepared by a coprecipitation method, as described in our previous report [17], using titanium sulfate solution (70 g/L TiO<sub>2</sub>, Tayca Corp.), silica sol (30 % SiO<sub>2</sub>, Nissan Chemical Corp.), ammonium molybdate (Taiyo Koko Co., Ltd.). TiO<sub>2</sub>-SiO<sub>2</sub> (TS) and TiO<sub>2</sub> were prepared similarly. The SiO<sub>2</sub> content in all TS and TSM samples was fixed to 7 wt%.

For comparison, MoO<sub>3</sub>/TS (Mo/TS) and MoO<sub>3</sub>/TiO<sub>2</sub> (Mo/TiO<sub>2</sub>) were prepared by an incipient wetness method. Ammonium molybdate (1.36 g) was mixed with monoethanol amine (0.55 g, Nippon Shokubai) and deionized water (5 g) at approximately 25 °C, and then the TS or TiO<sub>2</sub> powders (10 g) were impregnated with this molybdenum solution and mixed well. The conditions and procedure for drying and calcination were the same as those employed for the TSM samples. The nomenclature used for the various samples is “XMo/TiO<sub>2</sub>”, “XMo/TS”, and “XTSM”, where X represents the molybdenum content calculated as the weight percentage of MoO<sub>3</sub>. The molybdenum content in TSM ranged between 5 and to 30 wt%, and those in Mo/TS and Mo/TiO<sub>2</sub> were 10 or 30 wt%. Honeycomb-shaped vanadium catalysts were prepared in accordance with our previous report [17]. Ammonium metavanadate was mixed with an aqueous solution of monoethanol amine and oxalic acid at approximately 25 °C. The TSM powders and the vanadium solution obtained above were mixed and kneaded under the continuous addition of water. The resultant blend was fed into an extrusion molding device and molded into a honeycomb monolith. After drying at 60 °C and then calcining at 450 °C for 5 h in air, a honeycomb catalyst with an outer diameter of 50 mm and a pitch of 3.2 mm was obtained.

V<sub>2</sub>O<sub>5</sub>-MoO<sub>3</sub>/TiO<sub>2</sub>-SiO<sub>2</sub> (V10Mo/TS) and V<sub>2</sub>O<sub>5</sub>-MoO<sub>3</sub>/TiO<sub>2</sub> (V10Mo/TiO<sub>2</sub>) were also prepared by the same method, with ammonium molybdate added to the mixed aqueous solution of ammonium metavanadate, monoethanol amine, and oxalic acid. V<sub>2</sub>O<sub>5</sub>/TiO<sub>2</sub>-SiO<sub>2</sub> (V/TS) was prepared by the same method as V10Mo/TS, except that no ammonium molybdate was added. The loading amount of vanadium on all the catalysts in the present study was fixed at 8 wt% V<sub>2</sub>O<sub>5</sub>.

### 2.2. Characterization of the catalysts

The X-ray diffraction (XRD) measurements of the support materials and catalysts were carried out using a Rigaku SmartLab diffractometer with a CuK<sub>α</sub> radiation source under ambient conditions. The specific surface areas of the samples were evaluated by the Brunauer-Emmett-Teller (BET) method using a Mountech Macsorb Model 1210 apparatus. The samples were degassed in flowing N<sub>2</sub> at 200 °C for 60 min.

X-ray photoelectron spectroscopy (XPS) spectra were obtained using a ULVAC PHI Quantera SXM instrument. The sample powders were

fixed on double-sided carbon tape on an Al stub. The spectra were recorded at 25 °C under a pressure of  $< 1.33 \times 10^{-6}$  Pa using an AlK<sub>α</sub> radiation source with a beam diameter of 100 μm and a pass energy of 140 eV. The binding energies were calibrated to the C1s peak.

The V K-edge XANES measurements were performed at the BL-9C beamline of the Photon Factory (KEK-PF). The sample masses were calculated to adjust the height of edge jump and mixed with boron nitride (catalyst sample:boron nitride = 1:11) before being pressed into an *in situ* cell to form a self-supporting disc with a diameter of 7 mm. Nitrogen gas was fed into the *in situ* cell and the data were collected in transmission mode using a Si(1 1 1) monochromator at ambient temperature (25 °C) or at 200 °C. The XANES spectra were analyzed with the ATHENA software.

The Mo K-edge XAFS measurements were carried out at the BL01B1 beamline of SPring-8 (Japan Synchrotron Radiation Research Institute) in transmission mode. A double-crystal Si(1 1 1) monochromator was used. The sample masses were calculated to adjust the height of edge jump and mixed with boron nitride (catalyst sample:boron nitride = 2:1). The Ti K-edge XAFS measurements were performed at the BL-9C beamline of the KEK-PF using a Si(1 1 1) monochromator. The samples were mixed with boron nitride at a sample:boron nitride ratio of 1:3. For the Mo and Ti K-edge XAFS measurements, each samples mixed with boron nitride was pressed to form a self-supporting disc with a diameter of 10 mm, and the XAFS spectra were recorded at ambient temperature (25 °C) and pressure. The Mo and Ti K-edge XAFS data were analyzed using the REX2000 software (Rigaku Co.).

The V, Mo and Ti K-edge XANES spectra were normalized to the edge jump, and the first derivative of the near-edge region was employed for determination of the edge absorption energy. The *k*<sup>3</sup>-weighted EXAFS oscillations of the Mo and Ti K-edges were extracted using spline smoothing. Subsequently, the filtered *k*<sup>3</sup>-weighted  $\chi(k)$  was Fourier transformed into R space (*k* range: 3–13 Å<sup>-1</sup>) using a Hanning function window [19].

### 2.3. Catalytic activity measurements

Oxidative degradation tests using *o*-chlorotoluene were conducted in a U-shaped tubular stainless-steel reactor with an inner diameter of 3.8 cm. The honeycomb catalyst to be tested was cut into 25 cells and loaded into the reactor. A reaction gas mixture consisting of 100 ppm *o*-chlorotoluene, 10 % O<sub>2</sub>, and 10 % H<sub>2</sub>O by volume and balanced with N<sub>2</sub> was supplied to the reactor. *o*-Chlorotoluene and H<sub>2</sub>O were supplied using two glass saturators controlled at 31 °C for *o*-chlorotoluene and 46 °C for H<sub>2</sub>O. The reaction gas flow rate was 0.6 Nm<sup>3</sup>/h and the gas hourly space velocity GHSV was 6000 h<sup>-1</sup>. The reaction was carried out overnight (~15 h) at each temperature, and the *o*-chlorotoluene concentrations before and after the reaction were analyzed by gas chromatography using a Shimadzu GC-14B instrument equipped with a Chromosorb column controlled at 140 °C. The concentrations were analyzed 3–5 times every 20 min, and after confirming the value to be almost constant, the average value was used for decomposition rate calculations. The CO and CO<sub>2</sub> concentrations in the gas were measured using a Horiba PG-250 gas analyzer.

**Table 1**  
BET specific surface areas of the support materials and V–Mo catalysts.

Sample	Composition	BET surface area / m <sup>2</sup> /g
TiO <sub>2</sub>	TiO <sub>2</sub> (anatase)	82
TS	93 wt% TiO <sub>2</sub> -7 wt% SiO <sub>2</sub>	163
30Mo/TiO <sub>2</sub>	30 wt% MoO <sub>3</sub> /TiO <sub>2</sub>	55
30Mo/TS	30 wt% MoO <sub>3</sub> /TS	102
10Mo/TiO <sub>2</sub>	10 wt% MoO <sub>3</sub> /TiO <sub>2</sub>	64
10Mo/TS	10 wt% MoO <sub>3</sub> /TS	124
30TSM	63 wt% TiO <sub>2</sub> -7 wt% SiO <sub>2</sub> -30 wt% MoO <sub>3</sub>	115
20TSM	73 wt% TiO <sub>2</sub> -7 wt% SiO <sub>2</sub> -20 wt% MoO <sub>3</sub>	122
10TSM	83 wt% TiO <sub>2</sub> -7 wt% SiO <sub>2</sub> -10 wt% MoO <sub>3</sub>	135
V10Mo/TiO <sub>2</sub>	8 wt% V <sub>2</sub> O <sub>5</sub> -10 wt% MoO <sub>3</sub> /TiO <sub>2</sub>	60
V10Mo/TS	8 wt% V <sub>2</sub> O <sub>5</sub> -10 wt% MoO <sub>3</sub> /TS	111
V/10TSM	8 wt% V <sub>2</sub> O <sub>5</sub> /10TSM	101

### 3. Results

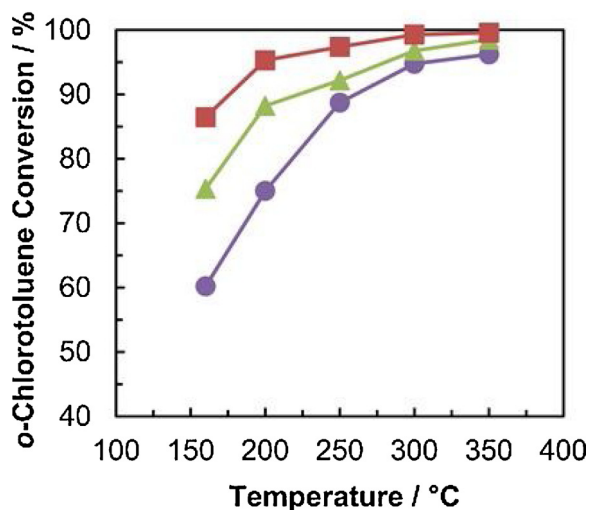
#### 3.1. Characterization of the supports and catalysts

Table 1 summarizes the BET specific surface areas of the support materials with various compositions and the corresponding V–Mo containing catalysts. TS and TSM were found to exhibit noticeably high specific surface areas (163 and 135 m<sup>2</sup>/g, respectively) compared to TiO<sub>2</sub> (82 m<sup>2</sup>/g), which was attributed to the presence of SiO<sub>2</sub> [3]. The surface areas of TS and 10TSM decreased when vanadium and/or molybdenum were added, but remained > 100 m<sup>2</sup>/g.

#### 3.2. *o*-Chlorotoluene oxidation activity

The results of the *o*-chlorotoluene oxidation reaction over three types of V–Mo catalysts are shown in Fig. 2. In the catalyst outlet gas, no organic compounds were detected with the exception of unreacted *o*-chlorotoluene, and it was confirmed that reacted *o*-chlorotoluene was converted to CO<sub>2</sub> by checking the carbon balance. The V/10TSM catalyst showed a significantly higher activity than the other two catalysts, especially at low temperatures.

Fig. 3 shows the performance of the catalysts with 8 wt% vanadium



**Fig. 2.** *o*-Chlorotoluene decomposition over V/10TSM (■), V10Mo/TS (▲), and V10Mo/TiO<sub>2</sub> (●). Reaction conditions: 100 ppm *o*-chlorotoluene, 10 vol% O<sub>2</sub>, 10 vol% H<sub>2</sub>O, N<sub>2</sub> balance; GHSV: 6000 h<sup>-1</sup>.

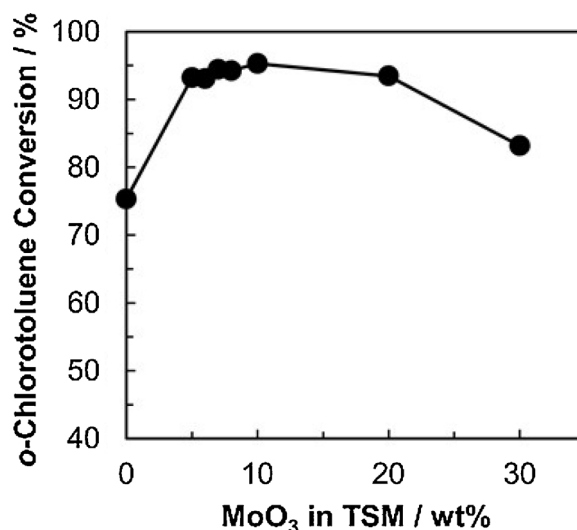


**Fig. 3.** *o*-Chlorotoluene decomposition over V/TSM as a function of MoO<sub>3</sub> loading. The reaction temperature is 200 °C and all other conditions are as described for Fig. 2.

supported on TSM containing different molybdenum contents, where the MoO<sub>3</sub> = 0 wt% data point corresponds to the performance of the V/TS catalyst. Notably, the catalytic activity is sharply enhanced upon the addition of 5 wt% molybdenum by the coprecipitation method. A gradual increase in catalytic activity is observed up to 10 wt%, but at higher molybdenum loadings, the activity decreases once again, thereby indicating that excess molybdenum inhibits the reactivity. Although the main active species in the *o*-chlorotoluene decomposition reaction is vanadium, it is clear that the activity strongly depends on the addition method and the amount of molybdenum.

#### 3.3. XRD

The XRD patterns of the catalysts and the support materials are shown in Fig. 4. In all samples, diffraction peaks ascribable to anatase TiO<sub>2</sub> (JCPDS: 00-021-1272) are observed. The XRD patterns of 30Mo/TiO<sub>2</sub> and 30Mo/TS display strong peaks assigned to  $\alpha$ -MoO<sub>3</sub> (JCPDS: 00-005-0508), and weak peaks at the same positions are observed for 10Mo/TiO<sub>2</sub> and 10Mo/TS (inset, Fig. 4). In contrast, the crystal phases of  $\alpha$ -MoO<sub>3</sub> and V<sub>2</sub>O<sub>5</sub> (JCPDS: 00-041-1426) are not detectable for the V10Mo/TiO<sub>2</sub> and V10Mo/TS catalysts. These observations suggest that the structure of molybdenum oxide is modified by interactions with vanadium in the V10Mo/TiO<sub>2</sub> and V10Mo/TS catalysts.

Furthermore, the XRD patterns of TSM display peaks ascribable to

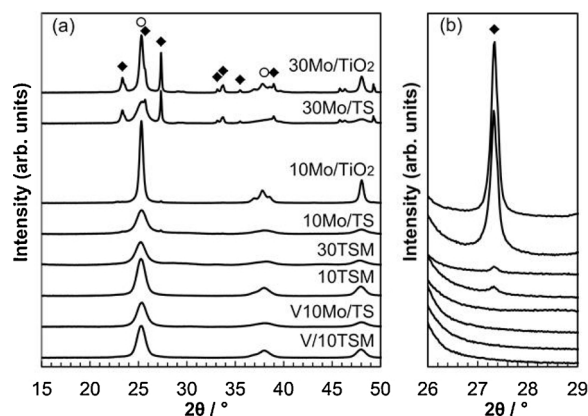


**Fig. 4.** (a) XRD patterns of the Mo-containing catalysts, and (b) enlarged data in the region of 26–29°. Symbols: MoO<sub>3</sub> (◆); TiO<sub>2</sub> (○).

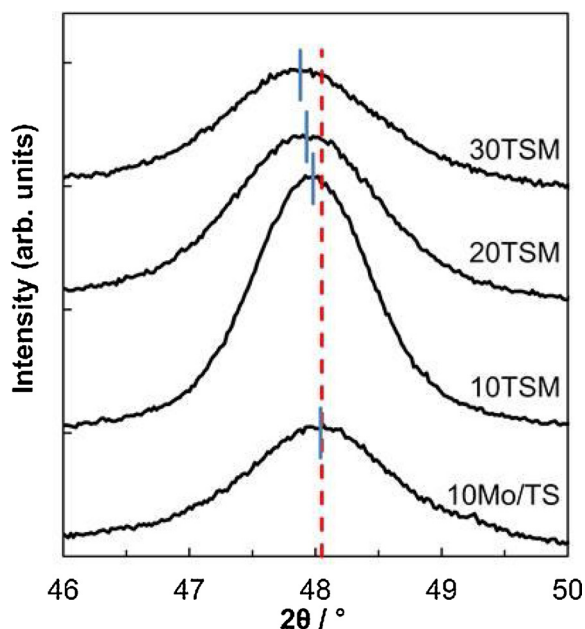


Fig. 5. Enlarged XRD patterns of the 10Mo/TS and TSM samples. The peak maxima for these samples (solid blue lines) and anatase TiO<sub>2</sub> (JCPDS No. 00-021-1272, dotted red line) are indicated (For interpretation of the references to colour in this figure legend, the reader is referred to the web version of this article).

anatase TiO<sub>2</sub> but do not display peaks corresponding to molybdenum oxide, even at a MoO<sub>3</sub> content of 30 wt% (30TSM). These results imply that the molybdenum species are highly dispersed within the TSM support.

As shown in Fig. 5, the diffraction peak observed at  $2\theta = 48^\circ$  for 10Mo/TS is consistent with that assigned to the (2 0 0) plane of anatase TiO<sub>2</sub>. A peak shift to lower diffraction angles is observed for TSM, with the extent of the shift increasing at higher molybdenum contents. The spacing between the (2 0 0) planes in the atomic lattice of 30TSM can be calculated as 1.900 Å (Table 2), which is clearly greater than that of anatase TiO<sub>2</sub> (1.892 Å).

### 3.4. XPS

The Mo-containing samples were characterized by XPS to investigate the properties of the surface molybdenum species (Fig. 6). The binding energies for Mo3d (232.6 eV) and Ti2p (458.7 eV) were identical in all samples, indicating that the majority of molybdenum and titanium species on the surface are present as Mo<sup>6+</sup> and Ti<sup>4+</sup>. The XPS Mo3d peaks of 10Mo/TiO<sub>2</sub>, 10Mo/TS and 10TSM, which are almost identical in shape, are broadened at lower binding energies compared to that of MoO<sub>3</sub>. This broadening can be attributed to the presence of another type of molybdenum species or to electron transfer between molybdenum and the support material [20]. These results indicate that the electronic features of the surface molybdenum species on 10TSM are similar to those on 10Mo/TiO<sub>2</sub> and 10Mo/TS.

Table 2

XRD peak positions and interplanar distances of the (2 0 0) plane of anatase TiO<sub>2</sub>.

	$2\theta / ^\circ$	Interplanar distance / Å
anatase TiO <sub>2</sub> (JCPDS)	48.05	1.892
10Mo/TS	48.04	1.894
10TSM	47.98	1.896
20TSM	47.92	1.898
30TSM	47.88	1.900

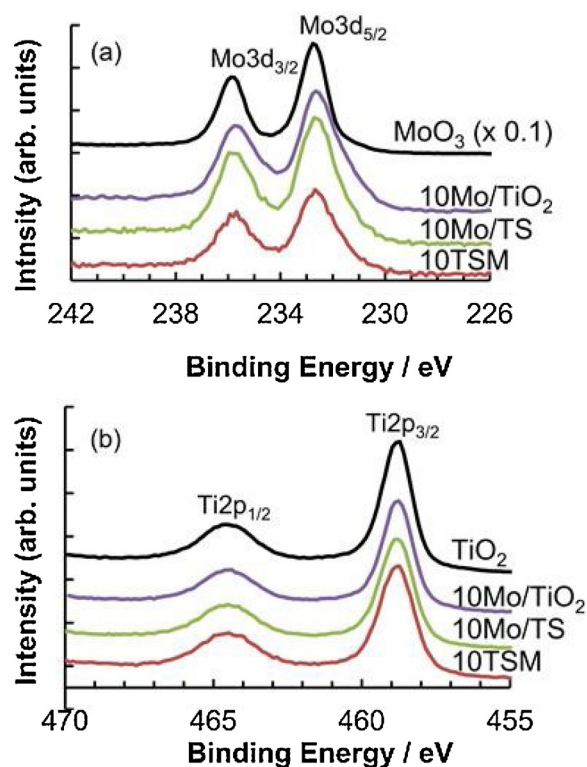


Fig. 6. (a) Mo3d and (b) Ti2p XPS spectra of the Mo-containing samples, normalized to the intensity of Ti2p<sub>2/3</sub> for comparison of the Mo/Ti ratio.

Table 3

Surface atomic compositions and Mo/Ti ratios estimated by XPS.

	Surface atomic composition / %				Mo/Ti
	Mo	Ti	Si	O	
10Mo/TiO <sub>2</sub>	8.0	28.2	–	63.8	0.29
10Mo/TS	6.8	25.5	4.0	63.8	0.27
10TSM	4.6	27.0	5.8	62.6	0.17

The surface compositions of these samples calculated from the XPS peak areas are summarized in Table 3. The surface atomic ratio of Mo/Ti for 10TSM is lower than those for 10Mo/TiO<sub>2</sub> and 10Mo/TS, thereby indicating that the surface molybdenum density on TSM is lower than those on the other supports, which suggests that molybdenum is incorporated within the particles.

### 3.5. V K-edge XANES spectroscopy

The V K-edge XANES spectra of the three vanadium catalysts as well as the V<sub>2</sub>O<sub>4</sub> and V<sub>2</sub>O<sub>5</sub> reference samples are presented in Fig. 7. For all samples, pre-edge peaks are observed at approximately 5468 eV. These peaks are observable due to the 3d–4p orbital mixing of vanadium, which is induced by the distortion of VO<sub>x</sub> from the octahedral VO<sub>6</sub> structure [21–23]. The pre-edge areas and main-edge positions are summarized in Table 4. As indicated, V<sub>2</sub>O<sub>5</sub> displays a larger pre-edge area than V<sub>2</sub>O<sub>4</sub>, suggesting a distorted square-pyramidal structure around the vanadium atom in V<sub>2</sub>O<sub>5</sub> [21–25]. The XANES spectra collected at 25 °C (thin line) and 200 °C (bold line) are identical for V<sub>2</sub>O<sub>4</sub> and V<sub>2</sub>O<sub>5</sub>. In contrast, the pre-edge and main-edge positions of the three catalysts shift to lower photon energies after heating to 200 °C, accompanied by a decrease in the pre-edge area. These results suggest that vanadium oxide is reduced to a lower oxidation state owing to the desorption of surface oxygen, and thus the morphology around the vanadium atom is altered. A greater shift is observed in the main-edge

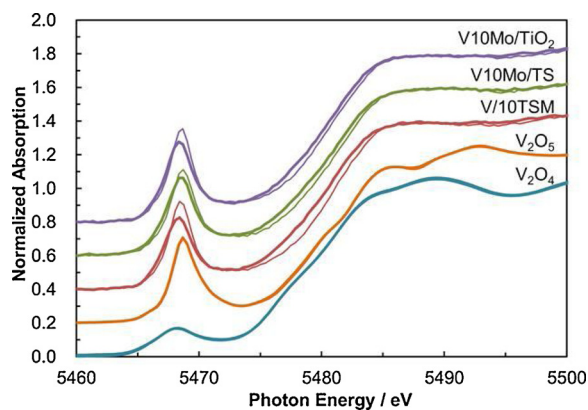


Fig. 7. Normalized V K-edge XANES spectra of the V-containing catalysts and reference samples collected at 25 °C (thin lines) and 200 °C (bold lines) under flowing N<sub>2</sub>.

Table 4

Pre-edge peak areas and main edge positions in the V K-edge XANES spectra.

	Pre-edge peak area		Main-edge position / eV	
	25 °C	200 °C	25 °C	200 °C
V <sub>2</sub> O <sub>4</sub>	0.96	0.99	5478.6	5478.5
V <sub>2</sub> O <sub>5</sub>	1.73	1.76	5480.0	5480.1
V10Mo/TiO <sub>2</sub>	1.81	1.75	5480.1	5479.7
V10Mo/TS	1.79	1.77	5480.1	5479.7
V/10TSM	1.74	1.65	5480.2	5479.5

position of V/10TSM than in those of V10Mo/TiO<sub>2</sub> and V10Mo/TS, indicating that the surface oxygen around vanadium is more easily desorbed over the V/10TSM catalyst. In other words, the reducibility of vanadium oxide is enhanced when supported on TSM.

### 3.6. Mo K-edge XANES spectroscopy

Fig. 8 displays the Mo K-edge XANES spectra of the molybdenum-containing samples and the molybdenum reference compounds (MoO<sub>2</sub>

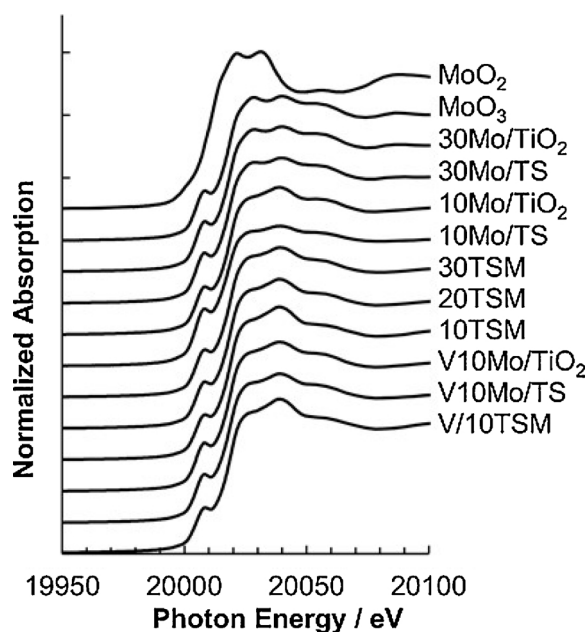


Fig. 8. Normalized Mo K-edge XANES spectra of the Mo-containing catalysts and reference samples.

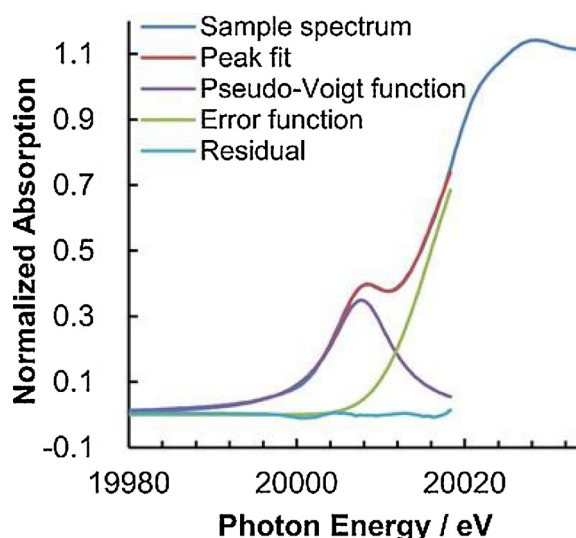


Fig. 9. Pseudo-Voigt fitting result for the normalized Mo K-edge XANES spectrum of MoO<sub>3</sub>.

and MoO<sub>3</sub>). All samples with the exception of MoO<sub>2</sub> exhibit pre-edge peaks, which can be observed due to the d-p orbital hybridization caused by the distortion of the octahedral MoO<sub>6</sub> structure [26–29]. For a quantitative analysis, the ATHENA software was used to fit the XANES spectra in this region with a pseudo-Voigt function in combination with an error function (Fig. 9). The absorption edge energies and pre-edge peak positions are the same as those of crystalline MoO<sub>3</sub>, indicating that molybdenum is present as Mo<sup>6+</sup>, regardless of the type of support, Mo loading amount, preparation method, or the presence of vanadium. Furthermore, 30Mo/TiO<sub>2</sub> and 30Mo/TS display similar pre-edge intensities to MoO<sub>3</sub>, which has distorted octahedral symmetry [26] (magnified spectra in Fig. 10). While 10Mo/TiO<sub>2</sub> and V10Mo/TiO<sub>2</sub> exhibit lower pre-edge intensities, 10Mo/TS demonstrates a higher pre-edge intensity than MoO<sub>3</sub>. It has been reported that MoO<sub>3</sub>/Al<sub>2</sub>O<sub>3</sub> catalysts exhibit intense pre-edge peaks, indicating the presence of a monomeric molybdenum oxide species [28]. This species seems to be highly dispersed owing to the large specific surface area of the Al<sub>2</sub>O<sub>3</sub> support. Therefore, the increased pre-edge intensity observed for 10Mo/TS can be attributed to the large specific surface area of the TS support, and it is likely that some molybdenum oxides on 10Mo/TS are present as monomeric species. In contrast, 30TSM demonstrates a lower pre-edge intensity than 10Mo/TiO<sub>2</sub>, and the intensity decreases as the molybdenum content decreases. According to the XRD results (Fig. 4), molybdenum atoms in TSM are more highly dispersed than those in Mo/TiO<sub>2</sub> and Mo/TS; however, monomeric molybdenum oxide species are not formed in the TSM samples, suggesting that the structure around molybdenum is less distorted.

The pre-edge intensity of the V10Mo/TS catalyst is clearly lower than that of 10Mo/TS, indicating the presence of an interaction between vanadium and molybdenum on V10Mo/TS. In the case of TSM, the pre-edges of 10TSM and V/10TSM are almost identical, indicating that the local symmetry around molybdenum in TSM is not affected by the presence of vanadium.

### 3.7. Mo K-edge EXAFS spectroscopy

The k<sup>3</sup>-weighted EXAFS spectra of the Mo K-edge and the corresponding Fourier transforms (radial structure function; RSF) of 30Mo/TiO<sub>2</sub> and 30Mo/TS are shown in Fig. 11, where the data of crystalline MoO<sub>2</sub> and MoO<sub>3</sub> are shown for reference. Intense peaks at 0.8–2.0 Å assigned to Mo–O are observed for all samples [28–31]. Furthermore, 30Mo/TiO<sub>2</sub> and 30Mo/TS exhibit EXAFS oscillations similar to those of crystalline MoO<sub>3</sub>, with a predominant peak at 3.0–4.0 Å owing to

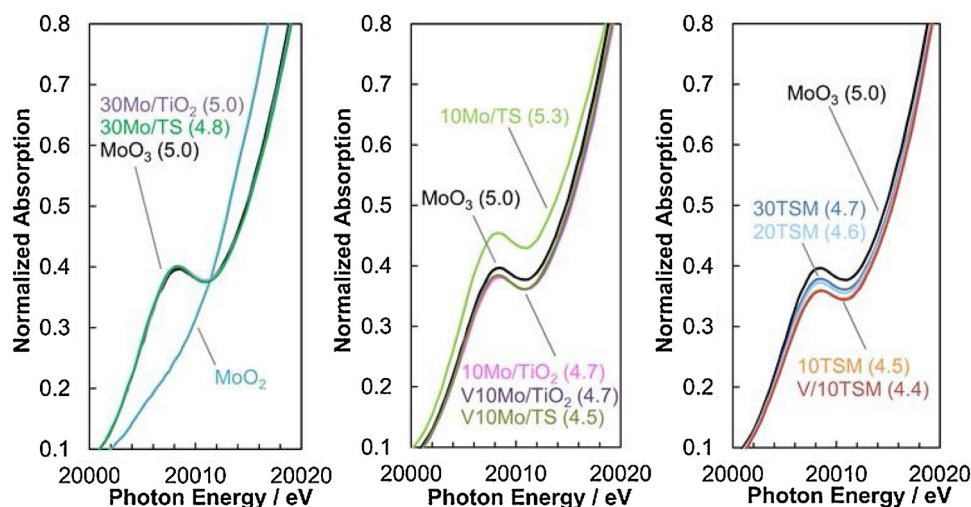


Fig. 10. Enlarged pre-edge regions in the normalized Mo K-edge XANES spectra. The values in parentheses are the pre-edge peak areas obtained by pseudo-Voigt fitting.

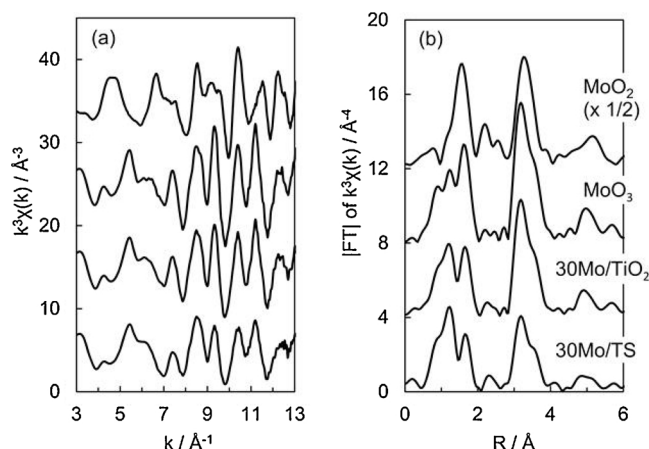


Fig. 11. (a)  $k^3$ -weighted Mo K-edge EXAFS spectra, and (b) corresponding Fourier transforms of the Mo-containing catalysts and reference samples.

Mo–Mo interactions. The majority of molybdenum oxides on these samples are found to be present as crystalline  $\text{MoO}_3$ , which is in good agreement with the XRD results.

The EXAFS oscillations and RSF of the samples containing 10 wt% molybdenum oxides either with or without vanadium and supported on  $\text{TiO}_2$  or TS are presented in Fig. 12. The EXAFS spectra and RSF of 10Mo/ $\text{TiO}_2$  and 10Mo/TS are quite different from those of crystalline  $\text{MoO}_3$ , and peaks are observed at approximately 2.4 and 3.0 Å. Although small peaks corresponding to  $\text{MoO}_3$  are observed in the XRD patterns (Fig. 4), the majority of molybdenum oxides have different structures to crystalline  $\text{MoO}_3$ . According to the literature concerning the EXAFS spectra of analogous  $\text{MoO}_3/\text{TiO}_2$  catalysts [32], the peaks observed at 2.0–3.5 Å for samples with lower molybdenum loadings are ascribable to Mo–Mo or Mo–Ti interactions.

The positions and intensities of the peaks observed in the 2.0–3.5 Å region of the RSF in Fig. 12 are summarized in Table 5. The amplitudes of peaks A and B in the RSF of 10Mo/TS are lower than those in the RSF of 10Mo/ $\text{TiO}_2$ , indicating a lower crystallinity and/or the presence of monomeric molybdenum species, as suggested by the XRD (Fig. 4) and XANES results (Fig. 10). Mensch et al. suggested that higher peaks close to 3 Å in the RSF of Mo K-edge EXAFS spectra reflect the polymerization of molybdenum species [28], thereby supporting the present results.

The Mo K-edge EXAFS spectra and the RSF of V10Mo/ $\text{TiO}_2$  and V10Mo/TS are similar to those of the samples without vanadium. A slight shift to shorter distances is observed for peak B after the addition

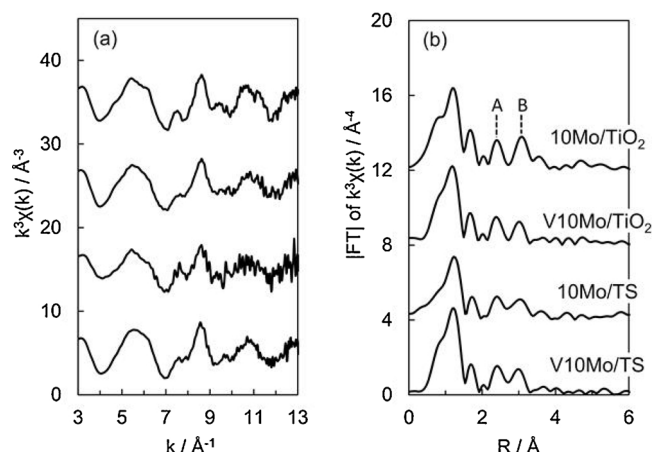


Fig. 12. (a)  $k^3$ -weighted Mo K-edge EXAFS spectra, and (b) corresponding Fourier transforms of the samples containing 10 wt% molybdenum oxide.

Table 5

Positions and intensities of peaks A and B in the RSF in Figs. 12 and 13.

	Peak A		Peak B	
	Position	Intensity	Position	Intensity
10Mo/ $\text{TiO}_2$	2.42	1.61	3.07	1.79
V10Mo/ $\text{TiO}_2$	2.38	1.51	2.99	1.25
10Mo/TS	2.42	1.25	3.03	1.10
V10Mo/TS	2.42	1.54	2.99	1.38
30TSM	2.42	1.34	2.95	1.63
20TSM	2.45	1.73	2.95	1.65
10TSM	2.53	2.29	2.88	2.22
V/10TSM	2.53	2.55	2.84	2.23

of vanadium. This change indicates the presence of interactions between vanadium and molybdenum, as suggested by the XRD and XANES results. The morphology around molybdenum seems to be altered by these interactions.

The EXAFS oscillations and RSF for TSM and V/10TSM are shown in Fig. 13. The EXAFS spectrum and RSF of 30TSM are similar to those of 10Mo/TS (Fig. 12), with peaks being observed close to 2.4 and 3.0 Å in the RSF. In accordance with the XRD results, it is confirmed that crystalline  $\text{MoO}_3$  is not formed in 30TSM.

Furthermore, changes in the EXAFS oscillations and RSF are

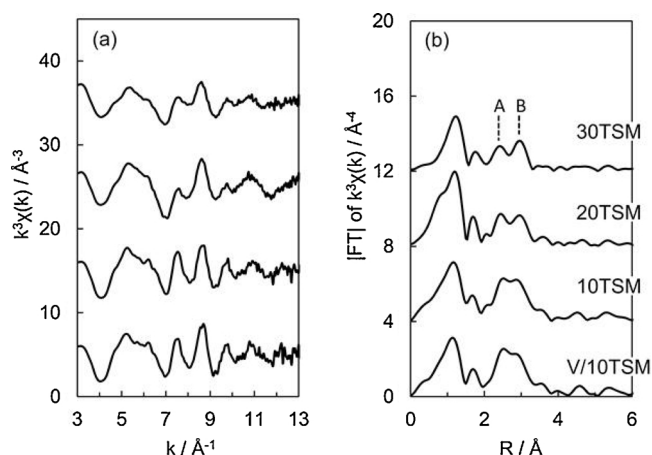


Fig. 13. (a)  $k^3$ -weighted Mo K-edge EXAFS spectra, and (b) corresponding Fourier transforms of the TSM and V/TSM samples.

observed as the molybdenum content decreases, and 10TSM shows a characteristic spectrum that is clearly different from those of  $\text{MoO}_2$ ,  $\text{MoO}_3$ ,  $\text{Mo/TiO}_2$ , and  $\text{Mo/TS}$ . The positions and intensities of peaks A and B in Fig. 13 are shown in Table 5. Shifts to longer distances for peak A and to shorter distances for peak B are observed, correlating to the molybdenum contents in the TSM sample. In addition, the amplitudes of peaks A and B increase with a decrease in the molybdenum content.

V/10TSM demonstrates an EXAFS spectrum similar to that of 10TSM, but peak B is shifted to a lower distance in the RSF. These results indicate that interactions between vanadium and molybdenum occur in the V/10TSM catalyst, similar to those in the other two V–Mo containing catalysts. However, the structure of 10TSM was mostly maintained following the addition of vanadium.

### 3.8. Ti K-edge EXAFS spectroscopy

The  $k^3$ -weighted EXAFS spectra of the Ti K-edge and the corresponding RSF of  $\text{TiO}_2$  and 10TSM are shown in Fig. 14, with the Mo K-edge EXAFS data for 10TSM and 10Mo/ $\text{TiO}_2$ . The  $\text{TiO}_2$  used as the support material for 10Mo/ $\text{TiO}_2$  has an anatase structure (confirmed by XRD, data not shown). The EXAFS oscillations in the Mo K-edge spectrum of 10TSM resemble those in the Ti K-edge EXAFS spectra of anatase  $\text{TiO}_2$  and 10TSM in the  $k$  range of 7–11.5  $\text{Å}^{-1}$  (dotted rectangle, Fig. 14a), suggesting that the Mo–Mo or Mo–Ti distances in 10TSM are very similar to the Ti–Ti distances in anatase  $\text{TiO}_2$ . This similarity is reflected in the RSF in the  $R$  range of 2–3  $\text{Å}$ , whereas the EXAFS spectrum and RSF of 10Mo/ $\text{TiO}_2$  in these ranges are obviously

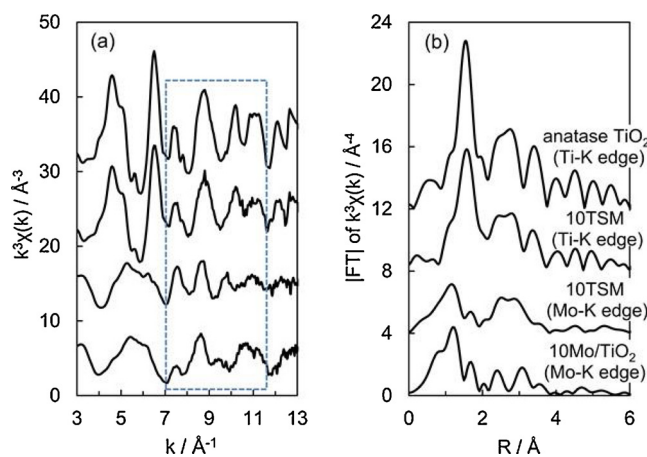


Fig. 14. (a)  $k^3$ -weighted Ti and Mo K-edge EXAFS spectra, and (b) corresponding Fourier transforms of 10TSM and  $\text{TiO}_2$ -based samples.

different from those of  $\text{TiO}_2$ .

## 4. Discussion

### 4.1. Structural characteristics of molybdenum in V/TSM catalysts

V/TSM catalysts, which are highly active for  $\text{NH}_3$ -SCR [17], also exhibit superior activity for the oxidative decomposition of *o*-chlorotoluene, especially at low temperatures (Fig. 2). The V10Mo/ $\text{TiO}_2$  catalyst showed the lowest activity, probably owing to its small surface area (Table 1). In contrast, the V/10TSM catalyst exhibited a higher activity than the V10Mo/TS catalyst, which had a higher surface area, thereby suggesting that the catalytic activity is affected by factors other than the surface area.

The V K-edge XANES spectra (Fig. 7) revealed that vanadium supported on TSM exhibits enhanced reducibility. Chang et al. suggested that the redox capability of vanadium is important for the oxidative decomposition of 1,2-dichlorobenzene [33]. Similarly, the redox capability of the vanadium species may contribute to the higher activity of V/TSM catalysts.

The major difference between V/10TSM and V10Mo/TS is the method for adding molybdenum. Therefore, the physicochemical properties of molybdenum in the V/TSM catalyst were investigated, and the XRD results showed that molybdenum is dispersed in the TSM support with a structure different from crystalline  $\text{MoO}_3$  (Fig. 4). The observed shift of the XRD peaks toward lower angles indicates an expansion of the interplanar distance brought about by the presence of molybdenum added by the coprecipitation method.

Moreover, as demonstrated by XPS, molybdenum is incorporated into the bulk structure of the TSM support, and no obvious differences are observed in the electronic behavior of the molybdenum species on the surface (Fig. 6). Mo K-edge XANES spectroscopy revealed that the oxidation state of molybdenum in V/10TSM is 6+ and that the octahedral structure around molybdenum is less distorted than in V10Mo/TS and V10Mo/ $\text{TiO}_2$  (Fig. 10). These results suggest that the electronic behavior of the surface molybdenum species has almost no influence on the catalytic activity for *o*-chlorotoluene decomposition.

In addition, the RSF data obtained from the Mo K-edge EXAFS spectra established that the Mo–Mo or Mo–Ti distances in the TSM support are different from those in crystalline  $\text{MoO}_3$ ,  $\text{Mo/TiO}_2$ , and  $\text{Mo/TS}$  (Figs. 11–13). In the RSF of 10TSM, the peaks A and B were located close to each other and the peak amplitudes were higher than those in other samples. These results imply that the structure of the V/10TSM catalyst is different from those of the other samples, and that 10TSM mostly consists of molybdenum oxide species with similar structures.

We attempted a curve-fitting analysis on the second shell contributions in the Mo K-edge EXAFS spectra. However, we could not obtain good fitting for the TSM-type samples because in this case, the second shell consists of more than two scatterings and we could not find an appropriate structural model for these peaks. Moreover, evaluation of the inverse Fourier transforms of the second shell did not reveal any significant difference between the TSM samples and 10Mo/TS, due to overlapping of plural EXAFS oscillations.

In contrast, according to past studies [34,35],  $\text{Ti}^{4+}$  (0.068 nm) in the lattice can be replaced by  $\text{Mo}^{6+}$  (0.062 nm), because they have similar ionic radii. Thus, molybdenum in the TSM support can be homogeneously incorporated into the TS framework as  $\text{Mo}^{6+}$ , forming a solid solution. Furthermore, the RSF of the Ti K-edge and Mo K-edge EXAFS spectra (Fig. 14) correspond to the second-shell contributions, and indicate that the Mo–Mo or Mo–Ti distances are very similar to the Ti–Ti distances in anatase  $\text{TiO}_2$ , strongly supporting the formation of a TSM solid solution.

#### 4.2. Influence of molybdenum oxides on the performance of V/TSM catalysts

The XRD and Mo K-edge XAFS analyses revealed the presence of V–Mo interactions in the V–Mo-containing catalysts, and it was found that the structural changes around molybdenum after the addition of vanadium were not remarkable for 10TSM (Figs. 10 and 13). However, the changes in the V K-edge XANES spectra after heating to 200 °C under flowing N<sub>2</sub> were most evident for V/10TSM (Fig. 7). These findings suggest that the superior catalytic activity of V/10TSM is the result of electronic interactions, mainly from the TSM support toward vanadium.

Tsai et al. reported that Mo-doped TiO<sub>2</sub> nanoparticles form a solid solution and that electron transfer from the support material to the active component is induced by oxygen vacancies generated in the nanoparticles [36]. It should be noted that the morphology around molybdenum in these Mo-doped TiO<sub>2</sub> nanoparticles was found to be tetrahedral, which is different from the octahedral structure of molybdenum oxide in the TSM support in the present study. This difference in structure is presumably ascribable to different preparation methods. However, similar to the case of Mo-doped TiO<sub>2</sub> nanoparticles, we believe that the electron transfer process is related to oxygen vacancies generated in the TSM solid solution.

While 30TSM exhibited a larger interplanar distance than 10TSM (Fig. 5), V/10TSM demonstrated a higher activity than V/30TSM (Fig. 3). These results indicate that the extent of electron transfer depends not on the total extent of distortion in the anatase TiO<sub>2</sub> framework, but on the local morphologies around molybdenum in the TSM support. Thus, electron transfer from the TSM support to vanadium is found to be enhanced when octahedrally coordinated molybdenum with a less distorted structure is well dispersed in the TSM support, in which Ti<sup>4+</sup> is replaced by Mo<sup>6+</sup>. The characteristics and unique structure of the TSM support contribute to enhancing the redox capability of vanadium in the V/TSM catalyst, resulting in a remarkable low-temperature *o*-chlorotoluene decomposition activity.

In our previous study [17], we reported that the V/TSM catalyst exhibits an improved NH<sub>3</sub>-SCR activity, which seemed to be related to the redox properties of V/TSM. The results in the present study are consistent with this hypothesis and enabled us to confirm it to be correct, with additional evidence for the role of the support material. Furthermore, it was found that the enhanced redox capability of V/TSM is also effective for the low temperature oxidative decomposition of *o*-chlorotoluene. As a result, the simultaneous decomposition of both NO<sub>x</sub> and dioxins can be achieved with a lower catalyst volume.

#### 5. Conclusions

We herein reported our investigation into the physicochemical characteristics of molybdenum oxide in V/TiO<sub>2</sub>–SiO<sub>2</sub>–MoO<sub>3</sub> (TSM) catalysts using X-ray diffraction (XRD), X-ray photoelectron spectroscopy (XPS), and X-ray absorption fine structure spectroscopy (XAFS), and their performance for the oxidative decomposition of *o*-chlorotoluene was examined. The V/TSM catalysts showed superior performance for the low-temperature oxidative decomposition of *o*-chlorotoluene, especially in the case of the TSM support containing 10 wt% molybdenum oxide. The vanadium species supported on 10TSM exhibited a higher reducibility, and this improved redox capability of vanadium is likely responsible for the enhanced catalytic activity. XRD, XPS, and Mo K-edge XAFS analyses revealed that the molybdenum present in the TSM support is octahedrally coordinated, with a less distorted structure than in the case of crystalline MoO<sub>3</sub>, and is also highly dispersed inside the TSM framework, thereby indicating the formation of a solid solution. Preparation of the TSM supports via a coprecipitation method appeared to result in the Ti<sup>4+</sup> within the TiO<sub>2</sub> structure being replaced by Mo<sup>6+</sup>. Electron transfer from the TSM support to the vanadium species was enhanced by the coexistence of

Mo<sup>6+</sup> and Ti<sup>4+</sup>, and thus the redox capability of the vanadium species supported on TSM was enhanced. However, the extent of electron transfer depended not on the total distortion of the anatase TiO<sub>2</sub> framework, but on the local morphologies around the molybdenum in TSM. Thus, the superior performance of the V/10TSM catalyst for the low-temperature decomposition of *o*-chlorotoluene was attributed to the high dispersion of Mo<sup>6+</sup> species in the 10TSM solid solution, which has a unique structure around molybdenum. This detailed physicochemical investigation provided insight into the structure of the TSM solid solution, and the enhanced redox capability of V/TSM was revealed to be effective for the low temperature oxidative decomposition of *o*-chlorotoluene. However, as the behaviors of the vanadium species and the support material during catalytic reactions have yet to be elucidated, future work in our group will focus on these points to contribute to the development of novel catalysts for improved NO<sub>x</sub> and dioxin abatement.

#### CRediT authorship contribution statement

**Ryoji Kuma:** Conceptualization, Methodology, Formal analysis, Investigation, Resources, Writing - original draft, Writing - review & editing, Project administration. **Tomoyuki Kitano:** Formal analysis, Investigation, Resources. **Takuya Tsujiguchi:** Investigation, Resources. **Tsunehiro Tanaka:** Writing - review & editing, Supervision.

#### Declaration of Competing Interest

The authors have no competing interests to declare.

#### Acknowledgements

We acknowledge Dr. K. Kimijima (High Energy Accelerator Research Organization, KEK) and Professor K. Okumura (Kogakuin University) for helpful and valuable assistance in the XAFS experiments. Publication permission and funding from Nippon Shokubai Co. Ltd. is also gratefully acknowledged.

#### References

- [1] L. Lietti, J. Svachula, P. Forzatti, G. Busca, G. Ramis, P. Bregani, Catal. Today 17 (1993) 131–139, [https://doi.org/10.1016/0920-5861\(93\)80016-T](https://doi.org/10.1016/0920-5861(93)80016-T).
- [2] G. Busca, L. Lietti, G. Ramis, F. Berti, Appl. Catal. B Environ. 18 (1998) 1–36, [https://doi.org/10.1016/S0926-3373\(98\)00040-X](https://doi.org/10.1016/S0926-3373(98)00040-X).
- [3] M. Kobayashi, R. Kuma, S. Masaki, N. Sugishima, Appl. Catal. B Environ. 60 (2005) 173–179, <https://doi.org/10.1016/j.apcatb.2005.02.030>.
- [4] J.-M. Herrmann, J. Disdier, Catal. Today 56 (2000) 389–401, [https://doi.org/10.1016/S0920-5861\(99\)00299-0](https://doi.org/10.1016/S0920-5861(99)00299-0).
- [5] I. Giakoumelou, C. Fountzoula, C. Kordulis, S. Boghosian, J. Catal. 239 (2006) 1–12, <https://doi.org/10.1016/j.jcat.2006.01.019>.
- [6] S.T. Choo, Y.G. Lee, I.-S. Nam, S.-W. Ham, J.-B. Lee, Appl. Catal. A Gen. 200 (2000) 177–188, [https://doi.org/10.1016/S0926-860X\(00\)00636-0](https://doi.org/10.1016/S0926-860X(00)00636-0).
- [7] S. Krishnamoorthy, J.P. Baker, M.D. Amiridis, Catal. Today 40 (1998) 39–46, [https://doi.org/10.1016/S0920-5861\(97\)00117-X](https://doi.org/10.1016/S0920-5861(97)00117-X).
- [8] S. Krishnamoorthy, M.D. Amiridis, Catal. Today 51 (1999) 203–214, [https://doi.org/10.1016/S0920-5861\(99\)00045-0](https://doi.org/10.1016/S0920-5861(99)00045-0).
- [9] M.A. Larrubia, G. Busca, Appl. Catal. B Environ. 39 (2002) 343–352, [https://doi.org/10.1016/S0926-3373\(02\)00116-9](https://doi.org/10.1016/S0926-3373(02)00116-9).
- [10] E. Finocchio, G. Busca, M. Notaro, Appl. Catal. B Environ. 62 (2006) 12–20, <https://doi.org/10.1016/j.apcatb.2005.06.010>.
- [11] D.P. Debecker, R. Delaigle, K. Bouchmella, P. Eloy, E.M. Gaigneaux, P.H. Mutin, Catal. Today 157 (2010) 125–130, <https://doi.org/10.1016/j.cattod.2010.02.010>.
- [12] C. Gannoun, R. Delaigle, D.P. Debecker, P. Eloy, A. Ghorbel, E.M. Gaigneaux, Appl. Catal. A Gen. 447–448 (2012) 1–6, <https://doi.org/10.1016/j.apcata.2012.08.034>.
- [13] M. Yu, W. Li, X. Li, X. Lin, T. Chen, J. Yan, Chemosphere 156 (2016) 383–391, <https://doi.org/10.1016/j.chemosphere.2016.05.011>.
- [14] C.E. Hetrick, J. Lichtenberger, M.D. Amiridis, Appl. Catal. B Environ. 77 (2008) 255–263, <https://doi.org/10.1016/j.apcatb.2007.07.022>.
- [15] G. Busca, M. Baldi, C. Pistarino, J.M. Gallardo Amores, V. Sanchez Escribano, E. Finocchio, G. Romezzano, F. Bregani, G.P. Toledo, Catal. Today 53 (1999) 525–533, [https://doi.org/10.1016/S0920-5861\(99\)00140-6](https://doi.org/10.1016/S0920-5861(99)00140-6).
- [16] M. Hiraoka, T. Fujii, K. Kashiwabara, K. Ieyama, M. Kondo, Chemosphere 23 (1991) 1439–1444, [https://doi.org/10.1016/0045-6535\(91\)90168-D](https://doi.org/10.1016/0045-6535(91)90168-D).
- [17] M. Kobayashi, R. Kuma, A. Morita, Catal. Lett. 112 (2006) 37–44, <https://doi.org/10.1007/s10562-006-0161-4>.

- [18] N. Sugishima, M. Kobayashi, *Shokubai* 43 (2001) 559–564.
- [19] S. Yamazoe, Y. Hitomi, T. Shishido, T. Tanaka, *J. Phys. Chem. C* 112 (2008) 6869–6879, <https://doi.org/10.1021/jp711250f>.
- [20] B.M. Reddy, B. Chowdhury, P.G. Smirniotis, *Appl. Catal. A Gen.* 219 (2001) 53–60, [https://doi.org/10.1016/S0926-860X\(01\)00658-5](https://doi.org/10.1016/S0926-860X(01)00658-5).
- [21] F. Amano, T. Tanaka, *Catal. Commun.* 6 (2005) 269–273, <https://doi.org/10.1016/j.catcom.2005.01.007>.
- [22] W.C. Vining, J. Strunk, A.T. Bell, *J. Catal.* 285 (2012) 160–167, <https://doi.org/10.1016/j.jcat.2011.09.024>.
- [23] J. Wong, F.W. Lytle, R.P. Messmer, D.H. Maylotte, *Phys. Rev. B* 30 (1984) 5596–5610, <https://doi.org/10.1103/PhysRevB.30.5596>.
- [24] K.L. Bøyesen, K. Mathisen, *Catal. Today* 229 (2014) 14–22, <https://doi.org/10.1016/j.cattod.2013.12.056>.
- [25] S. Takenaka, T. Tanaka, T. Yamazaki, T. Funabiki, S. Yoshida, *J. Phys. Chem. B* 101 (1997) 9035–9040, <https://doi.org/10.1021/jp9716086>.
- [26] H. Aritani, T. Tanaka, T. Funabiki, S. Yoshida, M. Kudo, S. Hasegawa, *J. Phys. Chem.* 100 (1996) 5440–5446, <https://doi.org/10.1021/jp9525245>.
- [27] K. Shimura, H. Kanai, K. Utani, K. Matsuyama, S. Imamura, *Appl. Catal. A Gen.* 283 (2005) 117–124, <https://doi.org/10.1016/j.apcata.2004.12.042>.
- [28] C.T.J. Mensch, J.A.R. Van Veen, B. Van Wingerden, M.P. Van Dijk, *J. Phys. Chem.* 92 (1988) 4961–4964, <https://doi.org/10.1021/j100328a028>.
- [29] R. Radhakrishnan, C. Reed, S.T. Oyama, M. Seman, J.N. Kondo, K. Domen, Y. Ohminami, K. Asakura, *J. Phys. Chem. B* 105 (2001) 8519–8530, <https://doi.org/10.1021/jp0117361>.
- [30] S. Takenaka, T. Tanaka, T. Funabiki, S. Yoshida, *J. Phys. Chem. B* 102 (1998) 2960–2969, <https://doi.org/10.1021/jp980134n>.
- [31] J.A. Wharton, D.H. Ross, G.M. Treacy, G.D. Wilcox, K.R. Baldwin, *J. Appl. Electrochem.* 33 (2003) 553–561, <https://doi.org/10.1023/A:1024911119051>.
- [32] M.J. Fay, A. Proctor, D.P. Hoffmann, M. Houalla, D.M. Hercules, *Mikrochim. Acta* 109 (1992) 281–293, <https://doi.org/10.1007/BF01242483>.
- [33] H.-Y. Chang, S.-P. Wang, J.-R. Chang, H.-S. Sheu, S.-G. Shyu, *Appl. Catal. B Environ.* 111–112 (2012) 476–484, <https://doi.org/10.1016/j.apcatb.2011.10.037>.
- [34] Y.J. Feng, C. Wang, W.R. Cheng, J.H. Huang, T.X. Zhao, Q.H. Liu, Z. Xie, Z.Y. Pan, S.Q. Wei, *J. Phys. Conf. Ser.* 430 (2013) 012090, <https://doi.org/10.1088/1742-6596/430/1/012090>.
- [35] H.W. Kang, S.B. Park, A.-H.A. Park, *Int. J. Hydrogen Energy* 38 (2013) 9198–9205, <https://doi.org/10.1016/j.ijhydene.2013.05.106>.
- [36] M.-C. Tsai, T.-T. Nguyen, N.G. Akalework, C.-J. Pan, J. Rick, Y.-F. Liao, W.-N. Su, B.-J. Hwang, *ACS Catal.* 6 (2016) 6551–6559, <https://doi.org/10.1021/acscatal.6b00600>.